Title

A taxonomy of site response complexity

Authors

Thompson, Eric M
Baise, Laurie G
Tanaka, Yasuo
et al.

Publication Date

2012-10-01

DOI

10.1016/j.soildyn.2012.04.005

Peer reviewed

Soil Dynamics and Earthquake Engineering 41 (2012) 32–43

Contents lists available at SciVerse ScienceDirect

Soil Dynamics and Earthquake Engineering

journal homepage: www.elsevier.com/locate/soildyn

A taxonomy of site response complexity

Eric M. Thompson [a,*], Laurie G. Baise [a], Yasuo Tanaka [b], Robert E. Kayen [c]

[a] Tufts University, 113 Anderson Hall, Medford, MA 02155, USA
[b] Research Center for Urban Safety and Security, Kobe University, Japan
[c] United States Geological Survey, USA

ARTICLE INFO

Article history:
Received 27 April 2011
Received in revised form
24 March 2012
Accepted 17 April 2012
Available online 31 May 2012

Keywords:
Soil properties
Seismic analysis
Seismic effects
Data analysis

ABSTRACT

A few extensively studied downhole seismic arrays are commonly used in detailed site response studies. Thus, there is a critical need to increase the number of sites that are used to compare soil constitutive models. Toward this end, we develop a classification scheme for downhole arrays that identifies stations where common wave propagation assumptions are valid. For stations where the one-dimensional (1D) assumption does not hold, we identify different levels of complexity that must be accounted for, which is a function of the inter-event variability and the similarity between the empirical and one-dimensional theoretical transfer functions. The classification is based on 100 seismic arrays in Japan that have recorded surface accelerations in excess of 0.3*g*, 69 of which exhibit low inter-event variability. The response at 16 of these sites resembles the one-dimensional response, while the others deviate from one-dimensional behavior, indicating that the one-dimensional assumption is not acceptable in most cases. We check our interpretation of the taxonomy with field investigations at two stations. The field observations show large lateral variations of the velocity profile across distances of hundreds of meters at the station where we expect the one-dimensional assumption does not hold.

1. Introduction

A fundamental task in engineering seismology is to separate the effects of the earthquake source, the path traveled by the various seismic waves, and the site where the ground motion is recorded. This is generally accomplished by assuming that each of these processes can be treated as a linear time invariant filter. The site effects are generally modeled as vertically propagating waves through the upper 100 m or so of soil and rock. Unfortunately the site effects can sometimes be influenced by more complex wave propagation, such as surface waves and scattering. This problem is exacerbated by the ambiguity that results because deviations from linear elasticity can have similar effects as linear path effects through heterogeneous crustal materials [1] and linear site effects through heterogeneous soils [2]. Downhole seismic arrays provide the most direct observations of dynamic soil behavior to remove the potential for confounding site effects with other seismic processes.

When chosen carefully and used with an appropriate wave propagation model, downhole seismic arrays provide valuable observations for calibration and validation of constitutive models. Downhole arrays do not necessarily isolate the underlying wave propagation assumptions from the constitutive model [3,4]. Thus, an additional step must be taken to ensure that the wave propagation assumptions are appropriate for each site. Toward this end, we present a taxonomy of downhole arrays that separates stations that should be used to validate one-dimensional nonlinear constitutive models from stations that require a more complex wave propagation model.

Many different methods with varying degrees of complexity have been employed to model the nonlinear response of geomaterials. For example, Frankel et al. [5] apply nonlinear correction factors to earthquake simulations. They consider three different techniques for applying nonlinear correction factors to the linear three-dimensional simulations: (1) the equivalent linear program SHAKE [6]; (2) the NEHRP amplification factors that are based on the time-averaged shear-wave velocity (V_S) in the upper 30 m of material (V_{S30}); and (3) the Choi and Stewart [7] amplification factions that are also a function of V_{S30}. The computer program SHAKE provides the most physically realistic of these three methods because the other two methods are based solely on empirical correlations. The limitations of SHAKE, however, include: (1) only vertically incident plane *S* waves are modeled; (2) nonlinear stress–strain behavior is approximated by the "equivalent linear" method; (3) lateral variations in the material properties are ignored; (4) pore pressure generation of saturated soils is ignored; and (5) inelastic strains are ignored.

Kwok et al. [8] compared five commonly used fully nonlinear codes to SHAKE in a blind test at the Turkey Flat downhole array

* Corresponding author. Tel.: +1 6176273098; fax: +1 6176273994.
E-mail address: eric.thompson@tufts.edu (E.M. Thompson).

0267-7261/$ - see front matter © 2012 Elsevier Ltd. All rights reserved.
http://dx.doi.org/10.1016/j.soildyn.2012.04.005

for the ground motion recorded from the 2004 **M** 6.0 Parkfield earthquake (the maximum acceleration at the Turkey Flat station was 0.29*g*). They found that all of these codes generally underestimate the site response amplifications at high frequencies (though the residuals still show trends at other frequencies). While the constitutive models of the different nonlinear codes vary, all of these codes assume vertically incident plane *S*-wave propagation through a laterally constant medium. The discrepancies between the different nonlinear codes and the observed ground motions could arise from: (1) errors in the assumed or estimated soil properties (e.g., modulus reduction curves and V_S profile); (2) the limitations of the constitutive model (e.g., whether or not the code accounts for inelastic strains), or (3) the wave propagation assumptions (e.g., whether or not the code allows nonvertical incidence). By increasing the number of sites, the variety of geologic settings, and the number of ground motions that we use for analyzing nonlinear site response, we will improve our understanding of how these different levels of complexity limit the accuracy of site response analysis.

We use the term "complex site response" to refer to any site response modeling strategy that tries to overcome any of the above standard modeling assumptions. For stations where the main source of error is the uncertainty of the estimated soil properties, an appropriate modeling approach is to apply the Assimaki et al. [9] method of inverting for the attenuation and velocity structure. For stations where the main source of error is the form of the constitutive model, a more flexible and realistic model should be sought. For example, if the velocity and attenuation structure is accurate but SHAKE cannot account for the nonlinear behavior, then a fully nonlinear code should be used. For stations where the main source of error is the influence of lateral heterogeneities, a three-dimensional nonlinear code must be used to overcome these errors. The taxonomic rules that we propose in this paper are intended to distinguish between the different potential sources of error. The goal is to avoid confounding errors, such as calibrating a one-dimensional constitutive model against ground motions that are significantly influenced by three-dimensional effects. Using 100 Kiban–Kyoshin network (KiK-net) surface–downhole pairs in Japan, we develop taxonomic rules that separate downhole seismic arrays into four categories based on inter-event variability and the complexity of the wave propagation model required to match ground motions from small events. This classification scheme does not require strong motions, and therefore is widely applicable to stations that have yet to experience strong shaking.

The most challenging class of soil response to model are those sites where the response varies significantly between events. Thus, the first step of the classification is to quantify the inter-event variability with a single parameter. Additionally, we quantify how well the response matches the linear one-dimensional response predicted by the in situ soil properties.

We investigate two stations in greater detail to validate the appropriateness of the taxonomy classes: at the first station, our taxonomy suggests the assumption of laterally constant layering is valid, but not at the second station. We test this interpretation of our classification by visiting these two sites and measuring the velocity profile at four locations in the vicinity of each (augmenting the existing profiles at each site). These data show that the lateral variations of the velocities are substantially larger at the site where the classification scheme suggests that the assumption of laterally constant layers is violated. For this site pair, we then demonstrate that these three-dimensional effects can result in significant overestimation of the site response amplifications for ground motions where nonlinear effects are negligible and that the effect of soil heterogeneity can be confounded with soil nonlinearity effects for strong shaking.

2. Data

Data from the KiK-net strong-motion network in Japan provides numerous surface–downhole station pairs that have recorded earthquakes over a wide range of magnitudes and peak ground accelerations [10]. KiK-net also provides the seismic velocity structure for each station, derived from surface-source downhole-receiver logging.

We analyze data from KiK-net stations that recorded a surface acceleration larger than 0.3*g*. The ground motion data include 4862 records from 1573 earthquakes at 104 different stations. Although we want to identify sites that have both linear and nonlinear motions to help constrain site response models, we only use linear motions in the classification scheme. Thus, the classification scheme can be applied to a site before strong motions have been recorded.

We filter this database with a number of data quality criteria. We keep only the records where the minimum signal-to-noise ratio is greater than five for the 0.5–20 Hz passband, reducing the number of records to 3714. We keep only the stations for which we have 10 or more linear records with the previously described signal strength criteria, where "linear" is defined as records for which the peak ground acceleration at the surface is less than 0.1*g*; Beresnev and Wen [11] showed that nonlinearity only becomes perceptible at peak ground accelerations of about 0.1–0.2*g* or greater. Three sites (IBUH03, RMIH05, and SZOH33) do not fulfill this criteria. Additionally, there is no published velocity profile for site NIGH01; so we do not include it in our analysis. This results in 100 surface–downhole pairs that meet the above basic data requirements.

3. Methods

Site response is generally represented as a ratio of a frequency-dependent measure of ground motion intensity between two locations $\mathbf{x}_1$ and $\mathbf{x}_2$. The intensity is typically either the response spectrum or the Fourier amplitude spectrum. At location $\mathbf{x}$, let $g(t,\mathbf{x})$ denote a ground motion function and $G(f,\mathbf{x})$ denote its amplitude spectrum, where t is time and f is frequency. In terms of the amplitude spectrum, the site response at location $\mathbf{x}_1$ relative to $\mathbf{x}_2$ is

$$a(f) = \frac{G(f,\mathbf{x}_1)}{G(f,\mathbf{x}_2)}. \quad (1)$$

The ground motion at $\mathbf{x}_2$ is referred to as the reference location, and its location relative to $\mathbf{x}_1$ must be considered carefully. A common scenario is for both locations to be at the free surface: $\mathbf{x}_1$ seated on soft sediments and $\mathbf{x}_2$ seated on rock. In this paper, however, we model surface–downhole seismic arrays, and so $\mathbf{x}_2$ is located some depth below $\mathbf{x}_1$. Given this definition, there is still an ambiguity in how $g(t,\mathbf{x}_2)$ is defined. It can be either the upgoing incident wavefield from the nonattenuating halfspace, or the full wavefield at $\mathbf{x}_2$, including both the upgoing wave and the downgoing wave that is reflected off of the free surface. When using recorded ground motions from downhole depths of the order of 100–200 m, as in this paper, it is nearly impossible to separate the upgoing and downgoing waves. Thus, we include both the upgoing and downgoing waves in the definition of $g(t,\mathbf{x}_2)$. We refer the interested reader to the more thorough discussions of the downgoing-wave effect in Shearer and Orcutt [12] and Thompson et al. [2]. If $a(f)$ is estimated from recorded ground motions, then we refer to it as the empirical transfer function (ETF) and if it is computed from a model, then we refer to it as a theoretical transfer function (TTF).

3.1. Theoretical transfer function

We evaluate the accuracy of site response models by comparing TTFs to ETFs. The most common assumptions for computing a TTF include: (1) the medium is assumed to consist of laterally constant layers overlying a nonattenuating halfspace; (2) wavefronts are assumed to be planar; (3) only the horizontally polarized component of the *S* wave (the *SH* wave) is modeled; (4) damping is assumed to be frequency-independent, and is quantified in this paper by the quality factor (Q). We refer to these collective assumptions as the SH1D site response model.

In geotechnical engineering applications energy dissipation is typically expressed by the equivalent viscous damping ratio ($\xi = 1/2/Q$) for a single-degree-of-freedom system with a viscous dashpot, known as a Kelvin–Voigt solid with viscosity η (which is proportional to the rate of shear strain). Frequency-independent damping is achieved by defining the viscosity as $\eta = G\xi/\pi/f$, where G is the shear modulus [13]. This viscoelastic model of soil damping is also used by SHAKE [6].

We compute the SH1D TTF with the Thomson–Haskell matrix method [14,15] as implemented by the program Nrattle, which is distributed with the Boore [16] ground motion simulation program SMSIM. This code gives identical results to SHAKE for constant modulus and damping values. In this paper, we assume vertical incidence unless otherwise noted. The input parameters of Nrattle include *S*-wave velocity (V_S), density (ρ), and the intrinsic attenuation of *S* waves (${}^{i}Q_s^{-1}$). Since we do not have in situ estimates of ρ, we use the procedure recommended by Boore [17] for estimating ρ from *P*-wave velocity (V_P), where V_P is reported by the surface-source downhole-receiver survey. We set V_S and ρ of the nonattenuating halfspace equal to the same values of the deepest measured layer to avoid spurious amplifications from an arbitrary impedance contrast at the bottom of the borehole.

We do not have site-specific estimates of ${}^{i}Q_s$. So we choose a value of ${}^{i}Q_s$ with a grid search. We consider values of ${}^{i}Q_s$ from 2.5 to 35 at intervals of 2.5 and choose the value with the lowest mean squared error (MSE), where the error is the difference between median ETF (defined in the next subsection) and the SH1D amplification for the assumed ${}^{i}Q_s$ for the f = 0.5–20 Hz passband. We evaluated the MSE from 0.5 to 20 Hz in 200 logarithmically spaced samples. The resulting values of ${}^{i}Q_s$ range from 5 to 35 with a median of 12.5 for the 100 sites in this study.

There is a long history of research on whether or not damping in soils is frequency dependent or independent (e.g., [18,19]). Although damping is typically assumed to be frequency independent, recent lab test results have quantified the frequency dependence of Q (e.g., [20–22]). Similarly, many researchers have observed frequency-dependent Q in the surface–downhole transfer function (e.g., [23–27]). Seismic scattering is clearly frequency dependent and contributes to the observed (total) damping [2,28]. Also, Kokusho and Mantani [29] showed that frequency-independent damping can result in unrealistically large accelerations in the base motion.

Kausel and Assimaki [30] pointed out that even when the material parameters are selected to be strain-compatible (SHAKE's equivalent linear approach), the damping at high frequencies is over-estimated and confining pressure effects are not modeled. Thus, they developed a SHAKE-like approach that fits a two-parameter function to the strain spectrum within each layer to account for the frequency-dependent viscoelastic parameters. Similarly, Yoshida et al. [31] noted that the equivalent-linear method both over-estimates damping at high frequencies and over-estimates the maximum shear strength. They demonstrate that these limitations can be at least partially overcome with frequency-dependent viscoelastic parameters, as implemented in the program FDEL. Other recent efforts to improve upon the equivalent-linear method with frequency-independent damping include Meng [32], who developed a method to incorporate frequency-dependent soil properties, but did not include strain-dependent effects. Park and Hashash [33] modified the equivalent-linear approach to account for frequency-dependent soil properties, thus providing a procedure to account for both frequency- and strain-dependent modulus and damping.

Since one of the main goals of this paper is to assess the accuracy of the most common site response modeling assumptions, we use the simple frequency-independent damping formulation because it is the most widely used approach. It should be kept in mind that we identify many sites with poor fit to these assumptions, and the damping formulation is one possible approach to improve the accuracy of the site response model. We would like to emphasize here that our data screening criteria removes large-strain records, as discussed in Section 2. Thus, misfit between theory and observation with these data should be mainly attributed to violations of the linear wave propagation theory assumed in the SH1D model (e.g., a one-dimensional medium, or frequency-independent damping).

3.2. Empirical transfer function

We assume that $a(f)$ follows a lognormal distribution, where $\mu_{\ln}$ is the mean of $\ln[a(f)]$. Thus, the median of $a(f)$ is given by

$$\hat{a}(f) = \exp[\mu_{\ln}]. \tag{2}$$

A maximum likelihood estimate for $\hat{a}(f)$ is

$$\hat{a}(f) = \exp\left(\frac{1}{n}\sum_{i=1}^{n} \ln[a_i(f)]\right), \tag{3}$$

where $a_i(f)$ is the $a(f)$ for the i=1,…,n ground motions. A maximum likelihood estimate for the standard deviation is

$$\sigma_{\ln}(f) = \sqrt{\frac{1}{n}\sum_{i=1}^{n}(\ln[a_i(f)] - \ln[\hat{a}(f)])^2}. \tag{4}$$

Rather than attempting to window the *S* wave, we compute the spectra of the surface and downhole recordings from the entire ground motion record. Although this contaminates our analysis with other arrivals, we prefer this method for our paper due to the large number of recordings that we include in our analysis. We compute the surface and downhole spectra from the two-dimensional (2D) complex time-series of the two orthogonal horizontal time histories following Steidl et al. [34] after applying a 5% cosine taper to the records. We then smooth the spectra with a 0.5 Hz triangular weighting function.

3.3. Response spectra

Response spectra are a convenient method for describing a ground motion in a form that is more meaningful from an engineering perspective. The response spectra S_a at oscillator period T is the maximum acceleration of a single-degree-of-freedom system with damping ratio ξ, to a base excitation [13]. All response spectra in this paper assume $\xi = 5\%$, and we assume that the base excitation is $g(t,\mathbf{x}_1)$ (the surface ground motion). To combine the two orthogonal horizontal components of the recorded ground motion, we compute an orientation-independent response spectra termed GMRotI50 by Boore et al. [35], which is easily computed with the Boore [36] Fortran programs. GMRotI50 is derived from the set of geometric means of the two horizontal components rotated to all possible orthogonal rotation

angles [35]. The S_a residuals are given by

$$S_a^r(T) = \ln[S_a^o(T)] - \ln[S_a^p(T)], \quad (5)$$

where $S_a^o(T)$ is the observed and $S_a^p(T)$ is the predicted $S_a(T)$. Thus, negative values of $S_a^r(T)$ indicate overpredictions while positive values indicate underpredictions. $S_a^o(T)$ is the response spectra computed from the recorded $g(t,\mathbf{x}_1)$ (surface ground motion). $S_a^p(T)$ is the response spectra computed from the predicted ground motion at the surface [$\hat{g}(t,\mathbf{x}_1)$]. We compute $\hat{g}(t,\mathbf{x}_1)$ from the inverse Fourier transform of

$$\hat{G}(f,\mathbf{x}_1) = a^*(f) \times G(f,\mathbf{x}_2), \quad (6)$$

where $\hat{G}(f,\mathbf{x}_1)$ is the predicted amplitude spectrum at the surface, $a^*(f)$ is the SH1D TTF, and $G(f,\mathbf{x}_2)$ is the amplitude spectrum of the downhole record.

3.4. Velocity characterization by surface waves

The *S*-wave velocity (V_S) profile measurements that we have collected include multiple spectral analysis of surface waves (SASW) [37] profiles at each site. SASW is a noninvasive method of measuring the V_S profile. The procedure measures the phase velocity of Rayleigh waves at a wide range of wavelengths, which is related to the V_S profile through a nonlinear and nonunique geophysical inversion. Thus, the most direct observations for the SASW test are the dispersion curves (a plot of Rayleigh wave phase velocity vs wavelength or frequency). The Rayleigh waves are generated by an electromechanical shaker that vertically loads the ground surface at discrete frequencies. We employ the Lai and Rix [38] Fortran subroutines to solve the nonlinear SASW inverse problem. This method uses the Hisada [39] algorithm to compute the Rayleigh wave phase velocity from the one-dimensional V_S profile (i.e., the forward problem), and the Constable et al. [40] inversion algorithm to select the smoothest V_S profile that accurately reproduces the empirical dispersion curve.

We use the SASW method to characterize the V_S profiles because the cost of multiple downhole surveys, which can achieve better resolution and precision, is prohibitive. Note that blind prediction site characterization studies have shown that SASW characterizations are reliable and sufficiently accurate for site response studies [41,42].

The goal for each SASW survey that we present in this paper is to measure the Rayleigh wave phase velocity at wavelengths that would characterize the V_S of the upper 40–50 m of the subsurface. Although the deeper V_S structure is important for site response analysis, we did not attempt to maximize the depth of exploration because of the inherent lateral averaging of the SASW procedure. Larger depths are sampled by longer wavelengths, which sample an increasingly large horizontal radius of the subsurface. This attribute may be advantageous in many circumstances where a site-wide average estimate of the V_S profile is desirable. But the purpose of these data is to identify lateral variations in the V_S structure, so the lateral averaging of the SASW method obscures our ability to resolve these fluctuations.

4. Site response taxonomy

We have developed a site response taxonomy that can be applied to linear ground motions recorded at downhole seismic arrays. This taxonomy is designed to separate sites that require a complex site response analysis from those where the standard assumptions are sufficient.

4.1. Inter-event variability

The first criteria that we propose is based on the inter-event variability of the ETF for linear motions. The variability in the ETF within a suite of small-strain motions represents uncertainties in the site response analysis that are independent of the nonlinear constitutive model. This variability could arise because the site effects may not be independent of the source and path effects. For example, this could occur where shallow earthquakes produce substantial surface waves while deep earthquakes do not. If a large amount of variability in the ETF is observed from one linear event to the next, then the site requires a three-dimensional nonlinear model that can handle a spatial domain large enough to encompass the site and source. Thus, such sites are the most challenging class of downhole arrays to model.

Fig. 1 plots the ETF at two sites to illustrate the range of inter-event variability. Site SMNH01 in Fig. 1(a) has a relatively large degree of variation from one event to the next, while IWTH05 in Fig. 1(b) is relatively consistent from one event to the next. The distinguishing characteristic is the width of the confidence interval. Thus, we use an average value of σ to quantify the inter-event variability.

Unfortunately, the specific criteria used to estimate the inter-event variability is necessarily arbitrary. We view our proposed criteria as only one potential method, and hope that future refinements will be suggested and subsequently adopted by the research community. In this paper we quantify the inter-event variability of the ETF as the median $\sigma_{\ln}$ (Eq. (4)) of the ETF between the first and fourth peaks of the SH1D transfer function (σ_i). The calculation of σ_i does not extend to frequencies above

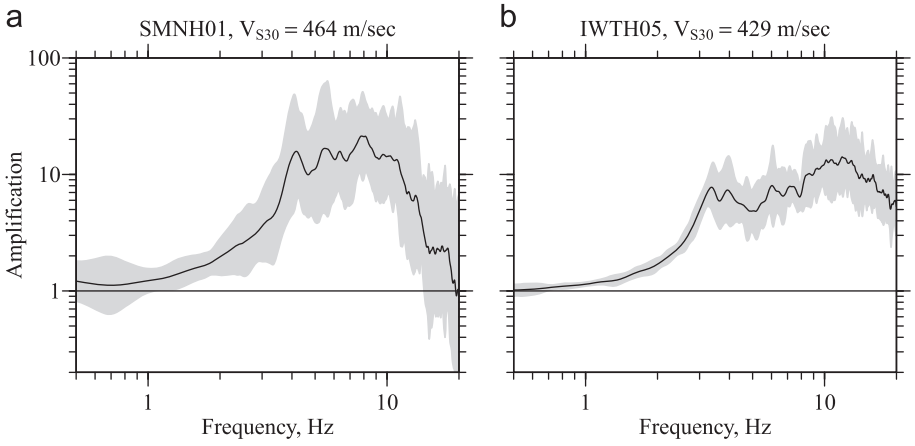

Fig. 1. The ETF at two stations: (a) SMNH01 is characteristic of a site with a large degree of inter-event variability and (b) IWTH05 is characteristic of a site with low inter-event variability.

20 Hz, even if the fourth peak is greater than 20 Hz. As it relates to Fig. 1, $\sigma_i = 0.50$ for SMNH01 and $\sigma_i = 0.28$ for IWTH05. We classify all sites as either "high σ_i" ($\sigma_i > 0.35$) or "low σ_i" ($\sigma_i < 0.35$). The exact cutoff value is debatable, but we feel that 0.35 is reasonable. Of the 100 stations in our database that fulfill the data quality criteria, 31 are classified as high σ_i.

4.2. Goodness-of-fit between SH1D and ETF

The second criteria that we propose is a goodness-of-fit metric between the SH1D and the ETF for linear ground motions. This is a measure of the validity of the SH1D assumptions, which are shared by most currently available nonlinear codes. The misfit between the ETF and the SH1D computation could arise from errors in the one-dimensional material properties [9] or from three-dimensional fluctuations of the material properties in space [2]. Fig. 2 gives two example sites to illustrate the range in goodness-of-fit between the SH1D and ETF. Site IBRH13 in Fig. 2(a) is a site where SH1D model accurately predicts the ETF, while site IWTH12 in Fig. 2(b) is a site where the SH1D does not match the ETF. The inter-event variability classification in the previous subsection labels both stations in Fig. 2 as low σ_i ($\sigma_i = 0.32$ for IBRH13; $\sigma_i = 0.26$ for IWTH12). Fig. 3 is an analogous figure, except that the two sites are classified as high σ_i: site IWTH04 in Fig. 3(a) is a site where the SH1D model accurately predicts the ETF, while site HRSH03 in Fig. 3(b) is a site where the SH1D does not match the ETF. Note that $\sigma_i = 0.354$ for IWTH04, which is very close to the high/low threshold.

Choosing an appropriate goodness-of-fit statistic requires consideration of what the different options measure. The mean-squared-error and the closely related coefficient of efficiency [43] are two commonly used measures of how close a model's predictions match observations. However, in this situation, we are less concerned with such measures of goodness of fit because they are fundamentally based on the square of the differences between the observed and predicted values. Here, we are concerned with the alignment of the resonances. The amplitude of the resonance peaks may not match because of the uncertainty of estimating the material damping. Thus, we choose to use Pearson's sample correlation coefficient r because it primarily measures whether or not the peaks are aligned.

Initial results using either arithmetically or logarithmically spaced samples from 0 to 20 Hz indicated that the r is strongly influenced by the average velocity of the site. The reason for this is that stiffer sites (with large V_{S30} values) have resonance peaks at higher frequencies. Thus, as V_{S30} increases, so does the percentage of the 0–20 Hz passband below the first peak in the transfer function. Frequencies below the first peak are

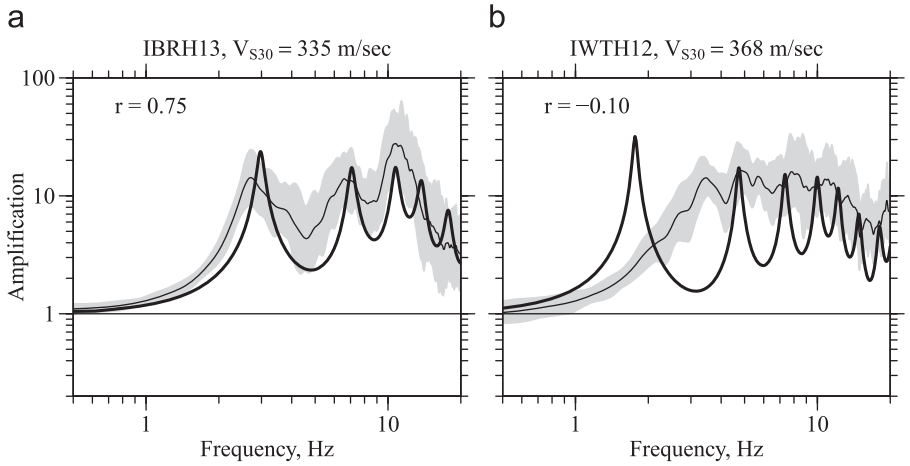

Fig. 2. The ETF and SH1D model at two stations: (a) IBRH13 is characteristic of a site where the SH1D model accurately predicts the ETF and (b) IWTH12 is characteristic of a site where the SH1D model poorly predicts the ETF. The goodness-of-fit statistics r is reported for each site, as described in the text.

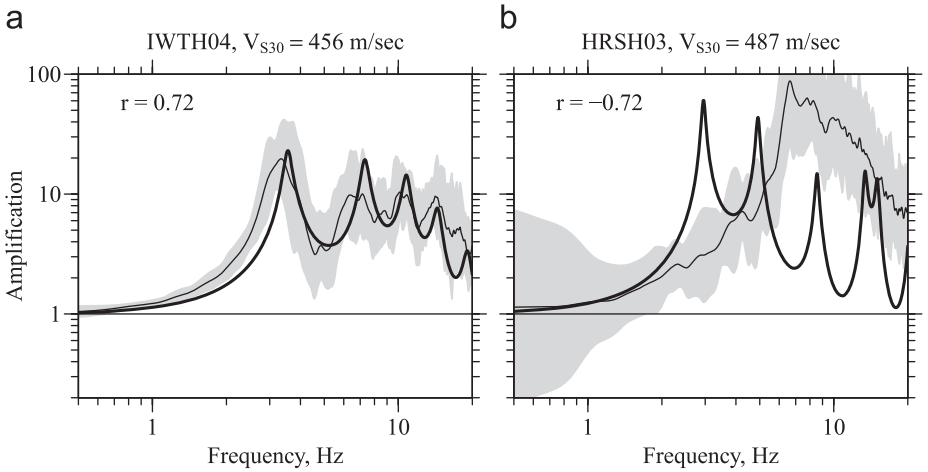

Fig. 3. The ETF and SH1D model at two stations where the inter-event variability of the transfer function is large: (a) IWTH04 is characteristic of a site where the SH1D model accurately predicts the ETF and (b) HRSH03 is characteristic of a site where the SH1D model poorly predicts the ETF. The goodness-of-fit statistics r is reported for each site, as described in the text.

characterized by a gradual monotonic increase in amplitude, and are not sensitive to the model input parameters. This results in an artificial dependence of r on V_{S30}. Thus, we feel that it is appropriate to exclude frequencies below the first peak from the computation of r. So we compute r for 200 logarithmically spaced frequencies between the first and fourth peaks in the SH1D transfer function. Through visual inspection of the SH1D and ETF curves along with the computed values of r, we choose to use a threshold value of $r > 0.6$ for sites classified as a "good fit to SH1D," and the remaining sites we classify as "poor fit to SH1D." Of the 100 stations in our database that fulfill the data quality criteria, 18 are classified as having a good fit to SH1D.

4.3. Taxonomy notation

To clearly and succinctly communicate the classification of a site, we use a two letter scheme. The first letter indicates the inter-event variability class (H for "high" and L for "low") while the second letter indicates the fit to SH1D (G for "good" and P for "poor"). Thus, all sites are separated into four distinct categories:

- LG sites have low σ_i and a good fit to SH1D. These sites are ideal for calibration and validation of one-dimensional constitutive models.
- LP sites have low σ_i and a poor fit to SH1D. These sites are appropriate for nonlinear modeling but care must be taken to identify the source of the misfit (e.g., soil heterogeneity, profile recalibration/optimization).
- HP sites have high σ_i, and thus they are not likely to be informative for nonlinear constitutive models unless path and source effects can be accounted for.
- HG sites are difficult to interpret because we would expect that if the inter-event variability is large, the fit to SH1D should be poor.

Fig. 4 plots σ_i and r as a function of V_{S30} and labels the respective cutoff values and the site response classifications. Fig. 4 shows that there are 16 LG sites with V_{S30} ranging from 144 m/s to 670 m/s and there are 53 LP sites that span an even wider range of V_{S30}. Table 1 summarizes the 100 sites that we use in this study, including the V_{S30}, the maximum depth of the velocity profile (Z_{max}; also the install depth of the downhole seismometer), the total number of linear events used to compute the ETF that meet our data quality criteria (n_{lin}), and the classification label for each site.

Table 1
Summary of the 100 KiK-net stations included in this study.

Station	V_{S30}, m/s	Z_{max}, m	n_{lin}	Class	Station	V_{S30}, m/s	Z_{max}, m	n_{lin}	Class
AKTH04	459	100	17	HP	EHMH02	489	110	24	LP
EHMH04	254	200	13	LP	EHMH05	362	134	30	HP
FKSH08	562	105	65	LP	FKSH09	585	200	50	HP
FKSH10	487	200	58	LP	FKSH11	240	115	33	LG
FKSH12	449	105	40	HP	FKSH14	237	147	43	LG
FKSH16	532	300	47	LP	FKSH18	307	100	63	LP
FKSH19	338	100	52	LP	FKSH21	365	200	32	HP
GIFH12	667	106	21	HP	GIFH22	807	100	18	LP
HRSH01	403	205	29	HP	HRSH02	391	100	24	HP
HRSH03	487	200	18	HP	HRSH07	461	102	24	HP
HYGH07	506	100	23	HP	IBRH10	144	900	61	LG
IBRH11	242	103	74	HP	IBRH12	486	200	54	LP
IBRH13	335	100	45	LG	IBRH14	829	100	62	HP
IBRH15	450	107	56	HP	IBRH16	626	300	65	LP
IBRH17	301	510	59	LG	IBRH18	559	504	50	LP
ISKH01	345	200	10	LP	ISKH02	721	102	15	LP
ISKH05	681	105	18	HP	ISKH09	636	106	29	HP
IWTH01	438	200	25	LP	IWTH02	390	102	15	LG
IWTH03	733	100	24	HP	IWTH04	456	106	21	HG
IWTH05	429	100	12	LP	IWTH07	396	120	31	LP
IWTH08	305	100	15	LG	IWTH09	967	100	16	HP
IWTH12	368	100	26	LP	IWTH14	816	100	19	LP
IWTH15	337	122	23	LP	IWTH17	1270	103	38	LP
IWTH18	892	100	18	LP	IWTH19	482	101	14	LP
IWTH20	289	156	15	LP	IWTH21	521	100	15	HP
IWTH22	532	100	44	LP	IWTH23	923	103	14	LP
IWTH24	486	150	19	LG	IWTH25	506	260	50	HP
IWTH26	371	108	14	LP	IWTH27	670	100	17	LG
KOCH05	1072	100	13	HP	KSRH02	219	105	16	LP
KSRH03	250	107	12	LP	KSRH04	189	240	84	LP
KSRH05	389	330	30	LP	KSRH06	326	237	24	LG
KSRH07	204	222	18	LG	KSRH09	230	100	22	LP
KSRH10	213	255	21	LG	MIEH05	590	100	10	HP
MIEH10	422	197	21	LP	MYGH02	399	203	25	LP
MYGH03	934	117	17	HP	MYGH04	850	100	21	LP
MYGH05	305	337	22	LP	MYGH07	366	142	18	LP
MYGH09	358	100	42	LP	MYGH10	348	205	25	LP
MYGH11	859	207	15	HG	NGNH18	379	100	21	HP
NGNH29	465	110	19	LP	NIGH06	336	100	52	HP
NIGH09	463	100	11	LP	NIGH11	375	205	14	LG
NIGH12	553	110	50	LP	NIGH14	438	387	14	LP
NMRH02	315	103	12	LP	NMRH04	168	216	18	LG
NMRH05	209	220	12	LP	OKYH14	710	100	14	LP
SMNH01	464	101	18	HP	SMNH02	503	101	15	HP
SZOH39	377	103	17	HP	SZOH42	153	203	18	LP
TCGH10	371	132	79	LP	TCGH11	329	200	64	LP
TCGH12	344	120	50	LG	TCGH13	574	140	67	LP
TCGH15	423	300	66	LP	TCGH16	213	112	50	LP
TKCH05	337	100	26	LP	TKCH07	140	100	23	LP
TKCH08	353	100	26	LG	TTRH02	310	100	20	HP

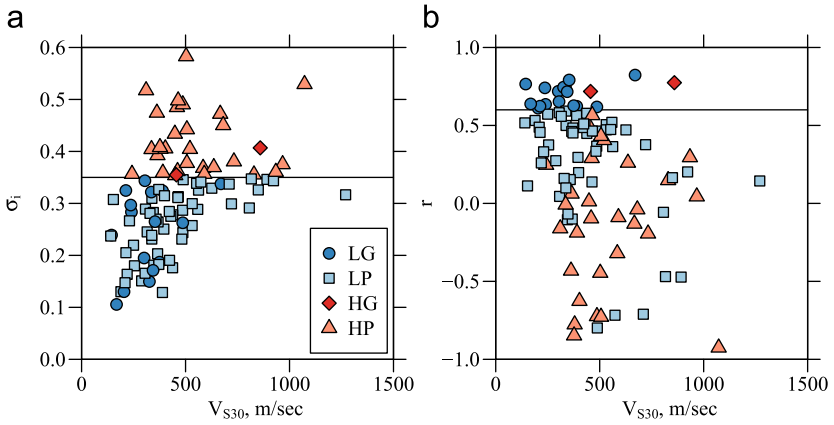

Fig. 4. (a) The inter-event variability (σ_i) and (b) the fit to SH1D (r) as a function of V_{S30} for the KiK-net sites.

5. Interpretation of taxonomy classes

We select a subset of the LG and LP sites as illustrative examples. Fig. 5 shows the ETF and SH1D amplifications for (a) TKCH08, (b) ISKH02, and (c) TKCH05. Site TKCH08 is a typical example of an LG site, with a narrow ETF confidence interval and the SH1D peaks closely aligned with the peaks observed in the ETF. The interpretation of the LG sites is the most straightforward: the standard modeling assumptions are appropriate. The interpretation of the LP sites (ISKH02 and TKCH05 in Fig. 5) requires more care.

Both of the LP sites in Fig. 5 have relatively narrow ETF confidence intervals and do not exhibit a good fit to the SH1D calculation. Note, however, that the nature of the misfit in sites ISKH02 and TKCH05 is distinctly different. The overall shape of the ETF at ISKH02 is similar to SH1D, but the first peak in the SH1D TTF is at a lower frequency than the first peak in the ETF. Thus, it is likely that a good fit of the SH1D model to the ETF could be achieved by increasing the velocities of the assumed horizontal layers or applying the Assimaki et al. [9] downhole seismogram inversion method. In contrast, the SH1D TTF and the ETF at TKCH05 are so dissimilar that no adjustment to the velocity profile will result in a satisfactory fit.

We first discuss possible explanations for the misfit at ISKH02, where we suspect that the one-dimensional model is still valid

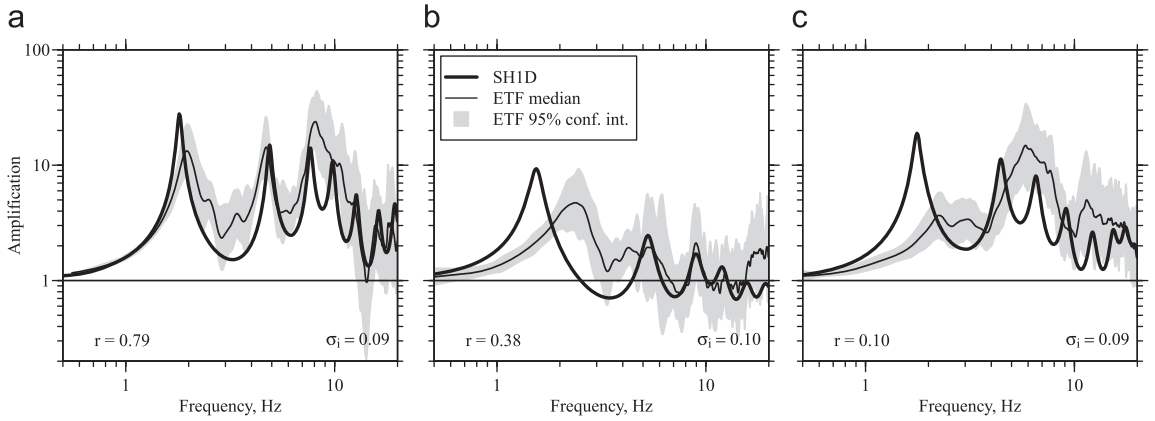

Fig. 5. The ETF and SH1D amplifications at sites (a) TKCH08, (b) ISKH02, and (c) TKCH05. The goodness-of-fit statistics r and the inter-event variability parameter σ_i are reported for each site. (a) V_{S30} = 353 m/sec, (b) V_{S30} = 721 m/sec and (c) V_{S30} = 337 m/sec.

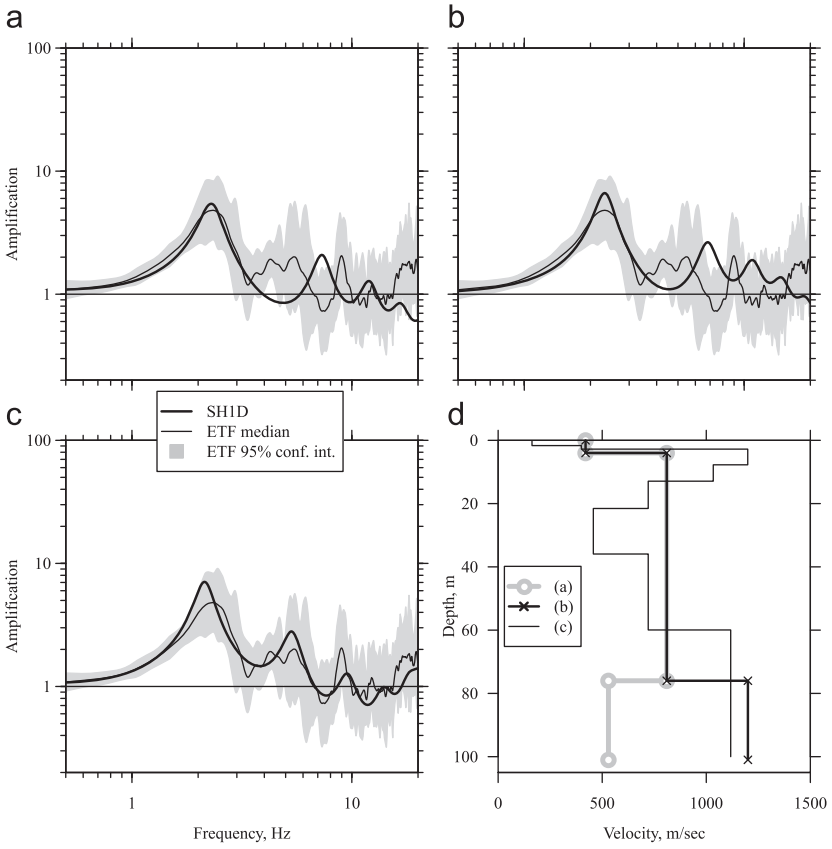

Fig. 6. ETF and SH1D amplifications at site ISKH02: The SH1D solution in (a) uses the downhole velocity structure with an incidence angle of 31° for the incoming *SH* waves, (b) increases the velocity of the bottom layer from 530 m/s to 1200 m/s and assumes vertically incident incoming waves, and (c) uses a more detailed velocity structure chosen to match the ETF as accurately as possible, assuming vertical incidence.

even though it is classified as an LP site. Multiple SH1D solutions offer substantial improvement over the SH1D solution with the measured downhole velocity structure at ISKH02, and we provide a few examples in Fig. 6. Subfigures (a)–(c) compare alternative SH1D solutions to the ETF and subfigure (d) gives the V_S profiles associated with each of these solutions. In Fig. 6(a), we use the original downhole velocity structure but increase the incidence angle from 0° (vertical) to 31° to match the frequency of the first peak to the ETF. This shifts all the peaks to higher frequencies and decreases the amplitudes. To match the amplitude of the first peak, we also increase ${}^{i}Q_s$ from 7.5 (for Fig. 5) to 10. Though we have improved the fit of the first peak, the other peaks to not match well. This is a "complex" model because nonvertical incidence is not typically considered in site response analysis. But a consistent incidence angle of 31° for many different events is unlikely and so this is not a satisfying solution.

An alternative solution strategy is to modify the layered velocity model. The velocities available at the KiK-net arrays are derived from surface-source downhole-receiver logging, and thus the velocities are based on travel time measurements, which are not typically associated with a large degree of uncertainty. To adjust the velocity profile, we must assume that these measurements or their interpretation is inaccurate. Ideally, we would inspect the recordings from which the travel time picks were taken. However, these data are not generally available. Here, we follow this approach to illustrate the multiple interpretations of the misfit between the ETF and SH1D at the site.

The uncertainty of the in situ velocity measurements increases with depth because the signal of the surface-source generally becomes more difficult to detect. Thus, we first attempt to increase the velocity of the bottom layer from 530 m/s (reported in the downhole profile) to 1200 m/s and assume ${}^{i}Q_s = 5$. The resulting amplifications are given in Fig. 6(b), and the V_S profile is displayed in Fig. 6(d) along with the original V_S profile reported by KiK-net. As with the SH1D result with increased incidence angle, the first peak matches the ETF, but the higher frequencies peaks are not aligned.

A third solution, represented in Fig. 6(c), has more layers (shown in Fig. 6d), and the velocities are adjusted so that the misfit between the ETF and SH1D is minimized. The velocities are optimized with a genetic algorithm [44]. The higher mode peaks match the ETF better than in the solutions in Fig. 6(a) and (b), though some accuracy of the first peak must be sacrificed to achieve the improvement at higher frequencies. The finer resolution profile also exhibits large fluctuations of the velocities that are not present in the original velocity profile. It is possible that these fluctuations have been averaged out by the coarse layering assumed in the downhole profile, and thus this "optimized" profile may be closer to the true properties of the soil. As we have demonstrated, the misfit could be due to a combination of

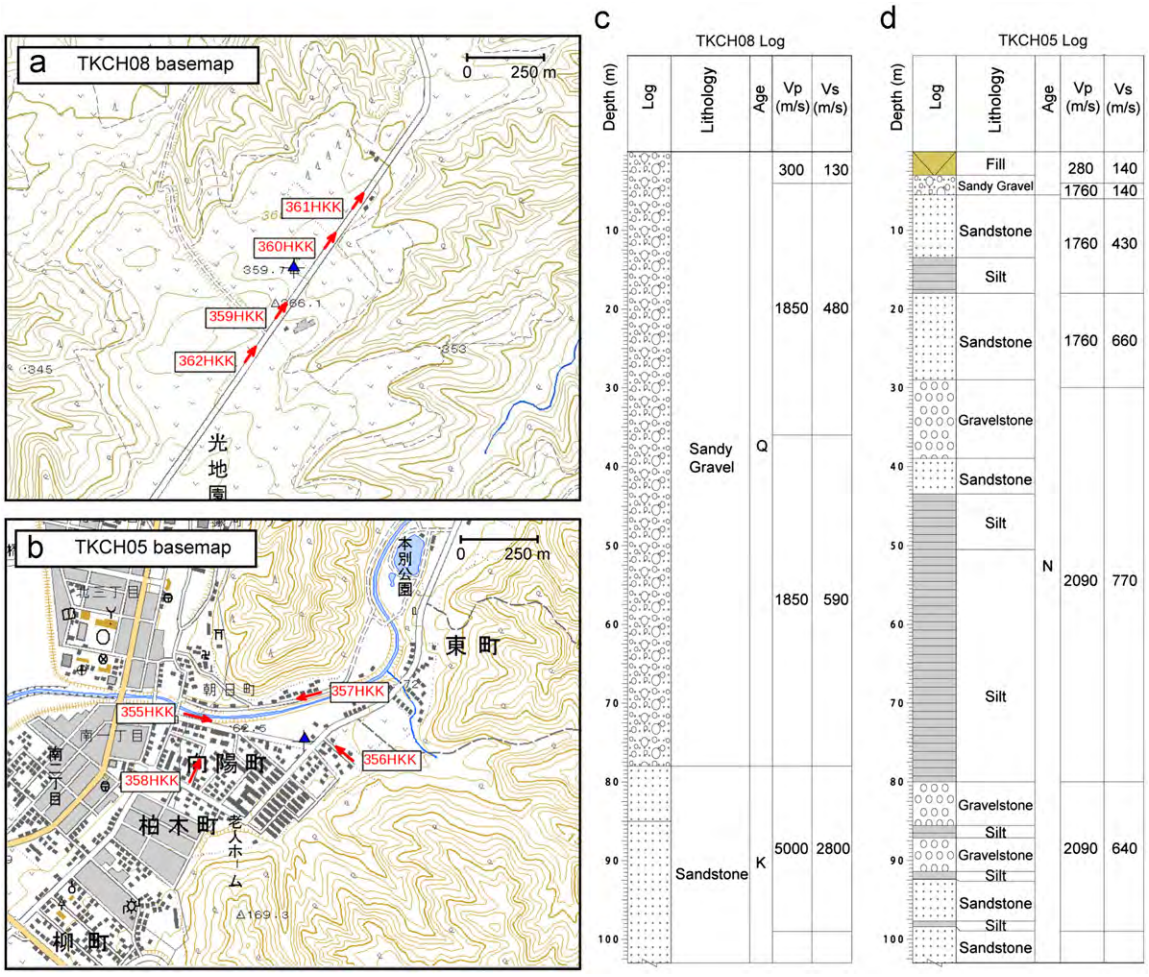

Fig. 7. Vicinity maps of KiK-net stations (a) TKCH08 and (b) TKCH05; and boring logs at stations (c) TKCH08 and (d) TKCH05. The vicinity maps show the location and orientation of the SASW surveys (red arrows) relative to the downhole arrays (blue triangles). The base of the red arrow identifies the location of the SASW seismic source, and the seismometer transect extends in the direction of the arrow. The length of the arrow indicates the distance to the furthest seismometer. The boring logs are modified from those available from the KiK-net website and include lithologic descriptions and the surface-source downhole-receiver velocity estimates. (For interpretation of the references to color in this figure caption, the reader is referred to the web version of this article.)

various simplifications or errors in the site response model, including (1) the assumption of vertical incidence, (2) bias in the V_S measurements, and (3) the limited resolution of the V_S profile.

In contrast to site ISKH02, no reasonable adjustment to the velocity profile at site TKCH05 (Fig. 5(c)) provides a satisfactory fit of the SH1D model to the ETF. The fundamental problem is that the ETF does not exhibit the destructive interference between the upgoing and downgoing waves that is predicted by the SH1D model (i.e., the downgoing-wave effect). Thus, we hypothesize that the source of the misfit at TKCH05 is due to lateral variations in the subsurface velocities that scatter the seismic waves and thus diminish the downgoing wave effect, as discussed by Thompson et al. [2] for site OKYH07.

6. Three dimension site effects

6.1. Identification of three-dimensional complexity at LP sites

Through comparisons of the two LP sites in Fig. 5, we have identified two different important sources of complexity in the site response analysis. Previously, we demonstrated that ISHK02 can still be explained with one-dimensional wave propagation; here we demonstrate that the misfit at TKCH05 arises because the one-dimensional assumption does not hold. To test the hypothesis that the main source of the misfit at site TKCH05 is due to three-dimensional wave propagation effects, we conduct four SASW surveys in the vicinity of both sites TKCH08 and TKCH05. If we are correct that the main source of the error at TKCH05 is lateral velocity variability, then we should see distinctly larger variability in the four SASW surveys in the vicinity of TKCH05 than TKCH08.

The vicinity maps and boring logs (including the lithologic descriptions and velocity estimates) for both stations are shown in Fig. 7. TKCH05 is in the town of Honbetsu while TKCH08 is located on a relatively isolated ridge. There are more potential testing locations at TKCH05, while access is limited to a single road at TKCH08. The spacing between the four different SASW surveys varied from 159 to 616 m at THCH08, and from 227 to 578 m at TKCH05. The red arrows indicate the layout of the SASW surveys in Fig. 7. The base of the arrow identifies the location of the electromechanical seismic source, and the length of the arrow approximates the distance that the receiver array extend away from the source.

The KiK-net downhole arrays are located at the blue triangles in Fig. 7(a) and (b). The descriptions of the lithology provided by the KiK-net website (Fig. 7(c) and (d)) provide preliminary evidence that TKCH05 may be more heterogeneous than TKCH08. The lithology at TKCH08 is relatively simple, consisting of 78 m of Quaternary sandy gravel over Cretaceous sandstone. In contrast, the top 80 m of TKCH05 consists of eight layers of Neogene deposits including fill, sandy gravel, sandstone, silt, and gravelstone. The stratigraphy below 80 m is mostly gravelstone and sandstone with thin interbeds of siltstone. The large velocities of the layers at TKCH05 indicate that the layers labeled silt are almost certainly siltstone (the discrepancy is easily attributed to the translation from Japanese to English).

The empirical and theoretical dispersion curves for each SASW survey at sites TKCH08 and TKCH05 are given in Fig. 8. The theoretical dispersion curves in Fig. 8 correspond to the inverted V_S profiles in Fig. 9. Fig. 9 also shows the KiK-net downhole

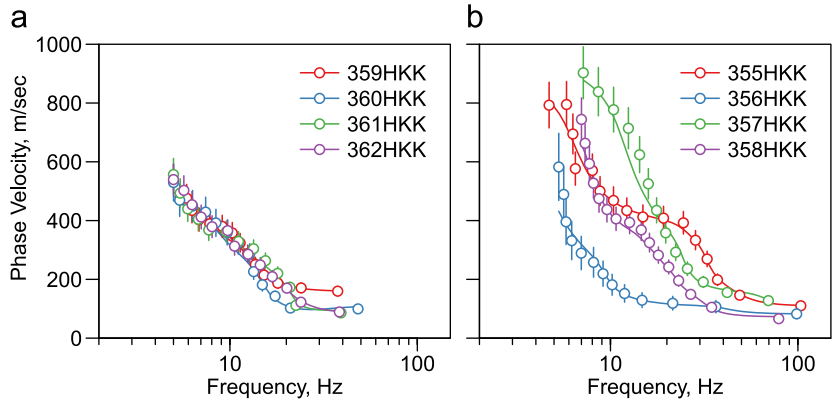

Fig. 8. Empirical (points) and theoretical (lines) dispersion curves near KiK-net (a) TKCH08 and (b) TKCH05.

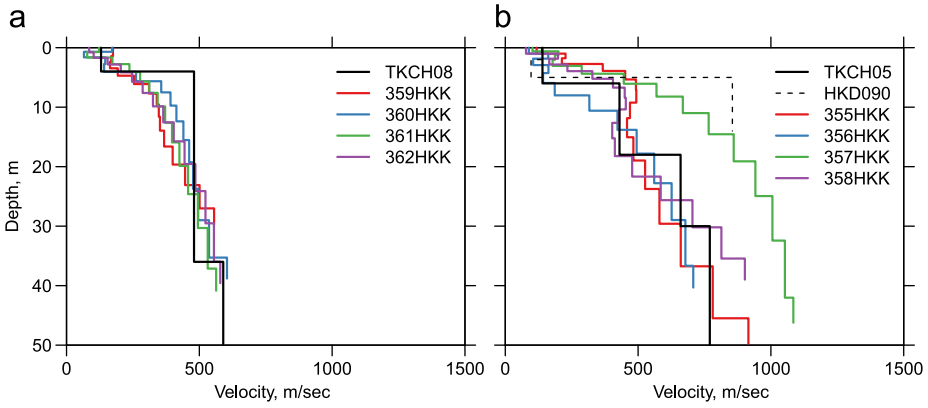

Fig. 9. Downhole and SASW V_S profiles near KiK-net sites (a) TKCH08 and (b) TKCH05.

profiles and the K-net profile at HKD090 because it is installed adjacent to TKCH05. Note that HKD090 is about 4 m from TKCH05, and so both stations are covered by the blue triangle in Fig. 7(b). The increased lateral variability of the in situ V_S profiles in the vicinity of the TKCH05 relative to TKCH08 supports our hypothesis that the misfit observed at TKCH05 in Fig. 5(c) is caused by three-dimensional spatial variability of the subsurface properties.

6.2. Evaluation of three-dimensional site response effects

Plots of the predicted and observed time histories are the most direct and intuitive method for assessing the performance of a ground motion model. However, such comparisons can be misleading because there is generally only space for a small subset of the ground motions in a single article and thus it is impossible to provide a comprehensive representation of the site behavior. Nevertheless, Fig. 10 illustrates the goodness-of-fit of the SH1D model for the East–West (EW) and North–South (NS) time histories at sites TKCH08 ((a) and (b)) and TKCH05 ((c) and (d)) for small amplitude ground motions.

As expected for small amplitude ground motions, the SH1D model predicts the surface motion relatively accurately at TKCH08 in Fig. 5 while a similarly small amplitude motion is substantially overpredicted at TKCH05. The overprediction at TKCH05 results because the SH1D model is compensating for the expected interference between the upgoing and downgoing waves at TKCH05, while the interference is not present in the observed ground motions. This demonstrates how the misfit in the transfer function (as displayed in prior figures) translates to the time histories that are easier to interpret from an earthquake hazards analysis perspective.

It is important to include both components and all of the ground motions when comparing predictions to observations because the goodness-of-fit varies substantially from one recording to the next and between the different components of the same recording. Thus, the data in Fig. 10 are for schematic demonstration, but general conclusions should not rely on a single observation such as this. Fig. 11 summarizes the performance of the SH1D model in terms of a $S_a^r(T)$ for sites TKCH08 and TKCH05. The shaded gray area is the 95% confidence interval of $S_a^r(T)$ for the linear events at each station. The black line is the $S_a^r(T)$ for the strong motion record at each site. It is interesting to note that at short periods ($T < 0.1$ s), the $S_a^r(T)$ have a similar pattern at the two sites in Fig. 11: the SH1D model generally underpredicts the ETF. However, at longer periods (0.5 s and greater), THKCH08 is generally unbiased, while the SH1D model for TKCH05 substantially overpredicts the ETF at the periods where the downgoing wave effect is expected by the SH1D TTF.

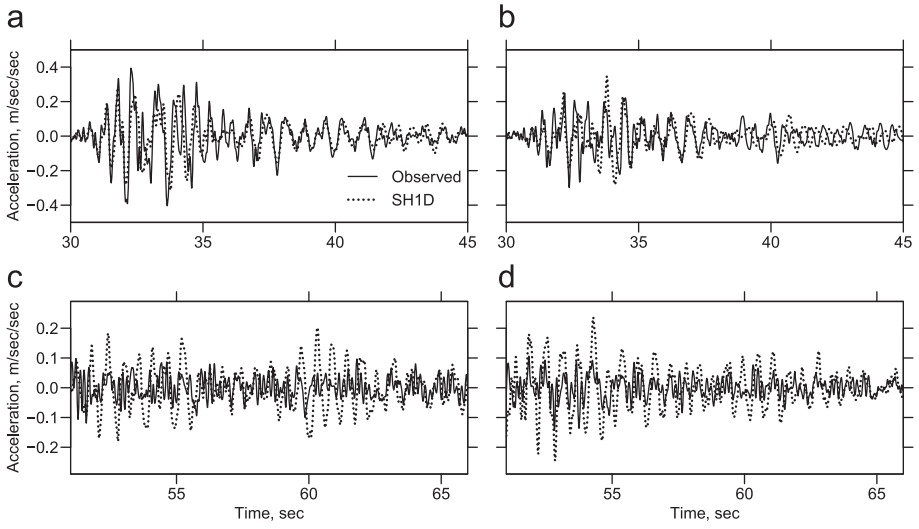

Fig. 10. Recorded and predicted surface EW and NS components of the ground motions at sites TKCH08 (a and b) and TKCH05 (c and d). The predicted surface records are computed from the downhole recording by applying the SH1D transfer function based on the downhole velocity structure. (a) TKCH08: EW and (b) TKCH08: NS.

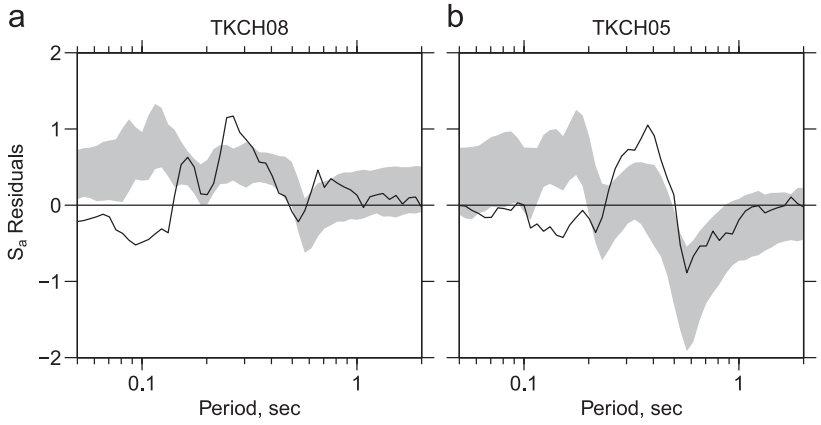

Fig. 11. Site response residuals at (a) TKCH08 and (b) TKCH05. The gray shaded region is the 95% confidence interval of the residuals for linear events, and the solid black line gives the residuals for the nonlinear event at each station.

7. Nonlinear effects

In the prior section, we discussed the differences in the $S_a^r(T)$ for TKCH08 and TKCH05 in Fig. 11 for linear events. Additionally, we see similar trends in the nonlinear effects for the strong motion that was recorded at these sites. Note that these comparisons are to show the level of misfit when we apply the viscoelastic SH1D model to motions that we expect to exhibit significant nonlinear effects. The strong motion at both sites are from the **M** 8.0 2003 Tokachi-Oki Earthquake. For this event, the peak acceleration at TKCH08 is 0.51*g* and at TKCH05 it is 0.41*g*. The residuals for the strong motion decrease at short periods relative to the linear events, indicating that S_a^o decreases because S_a^p remains constant for SH1D. Also, there is an increase in the residuals at intermediate periods (near 0.3 s) relative to the linear events, indicating that S_a^o increases. The differences between the residuals of the mainshock and the linear events, however, are generally smaller than the largest linear residuals at TKCH05. This indicates that complex linear wave propagation effects can be at least as important as nonlinear effects, at least for the sites and records that we consider here.

Reliable calibration and validation of constitutive models requires many case studies, and these case studies should ideally sample a realistic range of model input parameters. However, only a few extensively studied downhole arrays are commonly used for calibration and validation of nonlinear models, such as the large-scale seismic test (LSST) site in Lotung, Taiwan [45–50]. Thus, there is a critical need to increase the number of sites that are commonly used for nonlinear calibration and validation of dynamic soil constitutive models. In this paper, we suggest that the 16 LG sites in Table 1 are ideal for such studies.

8. Summary

We propose a site response classification scheme for surface–downhole strong motion arrays. This taxonomy is designed to identify those sites that require more complex analysis than the standard site response assumptions. This classification scheme is the key to expand the number of sites where nonlinear site response models are calibrated and validated.

Of the four categories that we propose, the most difficult to interpret is the HG class. Only two of the 100 sites in Table 1 are HG, one of which is IWTH04 in Fig. 3(a). The HG sites have a large amount of inter-event variability, but the median ETF matches the SH1D TTF relatively well. These sites are difficult to interpret because it seems unlikely that a site where the inter-event variability is large may produce a good overall fit.

We have identified 16 LG sites (low inter-event variability and good fit to SH1D) that are appropriate for calibration and validation of nonlinear site response models using standard SH1D assumptions. These sites range from deep soil sites to weathered rock sites, and will therefore provide an appropriate range of conditions for calibrating and validating soil constitutive models.

We have identified 53 LP sites that can be used for calibration and validation of more complex site response models. Such models should address issues such as nonvertical incidence, optimization of the soil profile, soil heterogeneity, earthquake source parameters, and full source-to-site waveform modeling. The KiK-net database is ideal for nonlinear site response studies because of the large number of stations that cover Japan, and the large earthquakes that this network has recorded. We find that many of the KiK-net sites are characterized by a large amount of inter-event variability that cannot be accounted for by currently available site-response modeling techniques. This underscores the need for the development of new methods that can relax some of the standard modeling assumptions.

Acknowledgments

This research is funded by National Science Foundation (NSF) Award #1000210. The Research Center for Urban Safety and Security at Kobe University hosted the first author which made this collaboration possible and funded the data collection presented in this article. Hidetaka Koumoto helped prepare the basemaps for stations TKCH08 and TKCH05. We thank Dr. Aoi and Prof. Kagawa for giving us the opportunity to inspect the detailed site investigation reports for the KiK-net stations. Comments by two anonymous reviewers and Ahmed Elgamal have improved this paper.

References

[1] O'Connell DRH. Replication of apparent nonlinear seismic response with linear wave propagation models. Science 1999;283(5410):2045–50.
[2] Thompson EM, Baise LG, Kayen RE, Guzina BB. Impediments to predicting site response: seismic property estimation and modeling simplifications. Bulletin of the Seismological Society of America 2009;99(5):2927–49.
[3] Bradley BA. A framework for validation of seismic response analyses using seismometer array recordings. Soil Dynamics and Earthquake Engineering 2011;31(3):512–20.
[4] Baise LG, Dreger DS, Glaser SD. The effect of shallow San Francisco Bay sediments on waveforms recorded during the Mw 4.6 Bolinas, California, earthquake. Bulletin of the Seismological Society of America 2003;93(1):465–79.
[5] Frankel AD, Stephenson WJ, Carver DL, Williams RA, Odum JK, Rhea S. Seismic hazard maps for Seattle, Washington, incorporating 3D sedimentary basin effects, nonlinear site response, and rupture directivity. U.S. Geological Survey Open-File Report 2007-1175; 2007. p. 77.
[6] Schnabel PB, Lysmer J, Seed HB. SHAKE: a computer program for earthquake response analysis of horizontally layered sites. Technical Report Rept. EERC 72-12, Earthquake Engineering Research Center, University of California, Berkeley; 1972.
[7] Choi Y, Stewart JP. Nonlinear site amplification as function of 30 m shear wave velocity. Earthquake Spectra 2005;21(1):1–30.
[8] Kwok AOL, Stewart JP, Hashash YMA. Nonlinear ground-response analysis of Turkey flat shallow stiff-soil site to strong ground motion. Bulletin of the Seismological Society of America 2008;98(1):331–43.
[9] Assimaki D, Steidl J, Liu PC. Attenuation and velocity structure for site response analyses via downhole seismogram inversion. Pure and Applied Geophysics 2006;163(1):81–118.
[10] Aoi S, Obara K, Hori S, Kasahara K, Okada Y. New Japanese uphole–downhole strong-motion observation network: KiK-Net. Seismological Research Letters 2000;72:239.
[11] Beresnev IA, Wen KL. Nonlinear soil response—a reality? Bulletin of the Seismological Society of America 1996;86(6):1964–78.
[12] Shearer PM, Orcutt JA. Surface and near-surface effects on seismic-waves—theory and borehole seismometer results. Bulletin of the Seismological Society of America 1987;77(4):1168–96.
[13] Kramer SL. Geotechnical earthquake engineering. Prentice Hall; 1993.
[14] Thomson WT. Transmission of elastic waves through a stratified solid. Journal of Applied Physics 1950;21:89–93.
[15] Haskell NA. The dispersion of surface waves on multilayered media. Bulletin of the Seismological Society of America 1953;72:17–34.
[16] Boore DM. SMSIM—Fortran programs for simulating ground motions from earthquakes: version 2.3. A revision of U.S. Geological Survey Open-File Report 96-80-A:55; 2005.
[17] Boore DM. Some thoughts on relating density to velocity 〈http://quake.wr.usgs.gov/~boore/daves_notes/daves_notes_on_relating_density_to_velocity_v1.2.pdf〉. 2008 [Accessed 24 April 2008].
[18] Hardin BO, Drnevich VP. Shear modulus and damping in soils: measurement and parameter effects. Journal of the Soil Mechanics and Foundations Division, ASCE 1972;98:603–24.
[19] Joyner WB, Chen ATF. Calculation of nonlinear ground response in earthquakes. Bulletin of the Seismological Society of America 1975;65(5):1315–36.
[20] Shibuya S, Mitachi T, Fukuda F, Degoshi T. Strain-rate effects on shear modulus and damping of normally consolidated clay. Geotechnical Testing Journal 1995;18(3):365–75.
[21] Rix G, Meng J. A non-resonance method for measuring dynamic soil properties. Geotechnical Testing Journal 2005;28(1):1–8.
[22] Khan ZH, Cascante G, El Naggar MH, Lai CG. Measurement of frequency-dependent dynamic properties of soils using the resonant-column device. Journal of Geotechnical and Geoenvironmental Engineering 2008;134(9):1319–26.

[23] Blakeslee S, Malin P. High-frequency site effects at 2 Parkfield downhole and surface stations. Bulletin of the Seismological Society of America 1991;81(2):332–45.
[24] Fukushima Y, Kinoshita S, Sato H. Measurement of Q-1 for S waves in mudstone at Chikura, Japan—comparison of incident and reflected phases in borehole seismograms. Bulletin of the Seismological Society of America 1992;82(1):148–63.
[25] Satoh T, Kawase H, Sato T. Evaluation of local site effects and their removal from borehole records observed in the Sendai region, Japan. Bulletin of the Seismological Society of America 1995;85(6):1770–89.
[26] Kokusho T, Aoyagi T, Wakunami A. In situ soil-specific nonlinear properties back-calculated from vertical array records during 1995 Kobe earthquake. Journal of Geotechnical and Geoenvironmental Engineering 2005;131(12): 1509–21.
[27] Kokusho T, Sato K. Surface-to-base amplification evaluated from KiK-net vertical array strong motion records. Soil Dynamics and Earthquake Engineering 2008;28(9):707–16.
[28] Sato T, Kawase H. Finite element simulation of seismic wave propagation in near-surface random media. In: Proceedings of international symposium on the effects of surface geology on seismic motion, Odawara; Japan 1992. p. 257–62.
[29] Kokusho T, Mantani S. Seismic amplification evaluation in a very deep downhole. In: 12th European conference on earthquake engineering; 2002 [Paper Reference 797].
[30] Kausel E, Assimaki D. Seismic simulation of inelastic soils via frequency-dependent moduli and damping. Journal of Engineering Mechanics 2002;128(1):34–47.
[31] Yoshida N, Kobayashi S, Suetomi I, Miura K. Equivalent linear method considering frequency dependent characteristics of stiffness and damping. Soil Dynamics and Earthquake Engineering 2002;22(3):205–22.
[32] Meng J. Earthquake ground motion simulation with frequency-dependent soil properties. Soil Dynamics and Earthquake Engineering 2007;27(3): 234–41.
[33] Park D, Hashash YMA. Rate-dependent soil behavior in seismic site response analysis. Canadian Geotechnical Journal 2008;45(4):454–69.
[34] Steidl JH, Tumarkin AG, Archuleta RJ. What is a reference site? Bulletin of the Seismological Society of America 1996;86(6):1733–48.
[35] Boore DM, Watson-Lamprey J, Abrahamson NA. Orientation-independent measures of ground motion. Bulletin of the Seismological Society of America 2006;94(4A):1502–11.
[36] Boore DM. TSPP—a collection of FORTRAN programs for processing and manipulating time series. U.S. Geological Survey Open-File Report 2008-1111.
[37] Nazarian S, Stokoe KH. In-situ shear wave velocities from spectral analysis of surface waves. In: Proceedings of the eighth world conference on earthquake engineering, vol. III. Englewood Cliffs, New Jersey: Prentice-Hall; 1984. p. 31–8.
[38] Lai CG, Rix GJ. Simultaneous inversion of Rayleigh phase velocity and attenuation for near-surface site characterization. Technical Report, Georgia Institude of Technology; 1998.
[39] Hisada Y. An efficient method for computing Green's functions for a layered half-space with sources and receivers close depths (part 2). Bulletin of the Seismological Society of America 1995;85:1080–93.
[40] Constable SC, Parker RL, Constable CG. Occams inversion—a practical algorithm for generating smooth models from electromagnetic sounding data. Geophysics 1987;52:289–300.
[41] Brown LT, Boore DM, Stokoe KH. Comparison of shear-wave slowness profiles at 10 strong-motion sites from noninvasive SASW measurements and measurements made in boreholes. Bulletin of the Seismological Society of America 2002;52:289–300.
[42] Boore DM, Asten MW. Comparisons of shear-wave slowness in the Santa Clara Valley, California, from blind interpretations of data from a comprehensive set of invasive and non-invasive methods using active- and passive-sources. Bulletin of the Seismological Society of America 2008;98: 1982–2003.
[43] Legates DR, McCabe GJ. Evaluating the use of "goodness-of-fit" measures in hydrologic and hydroclimatic model validation. Water Resources Research 1999;35(1):233–41.
[44] Mebane WR, Sekhon JS. Genetic optimization using derivatives: the rgenoud package for R. Journal of Statistical Software 2011;42(11):1–26.
[45] Elgamal AW, Zeghal M, Tang HT, Stepp JC. Lotung downhole array 1. Evaluation of site dynamic properties. Journal of Geotechnical and Geoenvironmental Engineering 1995;121(4):350–62.
[46] Lee CP, Tsai YB, Wen KL. Analysis of nonlinear site response using the LSST downhole accelerometer array data. Soil Dynamics and Earthquake Engineering 2006;26(5):435–60.
[47] Salvati LA, Pestana JM. Small-strain behavior of granular soils. II: seismic response analyses and model evaluation. Journal of Geotechnical and Geoenvironmental Engineering 2006;132(8):1082–90.
[48] Borja R, Sun W. Estimating inelastic sediment deformation from local site response simulations. Acta Geotechnica 2007;2:183–95, http://dx.doi.org/10.1007/s11440-007-0044-x.
[49] Reyes DK, Rodriguez-Marek A, Lizcano A. A hypoplastic model for site response analysis. Soil Dynamics and Earthquake Engineering 2009;29(1): 173–84.
[50] Tsai CC, Hashash YMA. Learning of dynamic soil behavior from downhole arrays. Journal of Geotechnical and Geoenvironmental Engineering 2009;135(6): 745–57.